RSC Advances

ROYAL SOCIETY OF CHEMISTRY

www.rsc.org/advances

Journal Name

ARTICLE

Carbon uptake during Spark Plasma Sintering: investigation through the analysis of the carbide "footprint" in a Ni-W alloy

Received 00th January 20xx,
Accepted 00th January 20xx

DOI: 10.1039/x0xx00000x

www.rsc.org/

B. B. Bokhonov,[a, b] A. V. Ukhina,[a] D. V. Dudina,[a, b, c] A. G. Anisimov,[c] V. I. Mali[c] and I. S. Batraev[c]

In the majority of studies of materials produced by Spark Plasma Sintering (SPS), the powders are consolidated in graphite dies using graphite punches and graphite protective foil. As a result, carbon uptake by the sintered material can take place. In this work, a Ni-15at.%W alloy was studied in this context for the first time and was chosen as a suitable model system, in which tungsten forms stable carbides while nickel does not, but offers a medium for carbon diffusion into the interior of the compact. In a disk-shaped 3-mm thick compact Spark Plasma Sintered at 900 °C, carbon uptake resulted in the formation of tungsten carbide WC particles ranging from 0.2 to 2 μm in the subsurface layers of the compact (within distances 50-100 μm from the interface with the foil). The size of WC particles varied with distance, smaller particles forming in the vicinity of the interface — in the area, in which the nucleation was favoured at high carbon concentrations. However, it was not only the subsurface layer that was affected by the presence of carbon: the particles of Ni_2W_4C were found at depths greater than 100 μm from the interface and throughout the volume of the compact. The distribution of the submicron WC particles and particles of Ni_2W_4C corresponded to a network of boundaries between the agglomerates of the Ni-W powder that was consolidated into a compact. These boundaries offered paths for faster diffusion of carbon from the foil compared with the volume of the agglomerates. The carbide subsurface layer dramatically changed the interdiffusion behaviour of the sintered material in a pair with aluminum due to a significantly reduced concentration of tungsten capable of diffusing within a metallic phase.

Introduction

Spark Plasma Sintering (SPS) is currently used in many laboratories worldwide and has become an attractive method of powder consolidation and solid-state synthesis [1]. Usually, the powders are consolidated using graphite dies and punches. In addition, graphite foil is used to ease the removal of the sintered sample from the tooling and is a popular material to protect graphite dies and punches from the chemical action of the specimen at elevated temperatures. All of the above act as planar sources of graphitic carbon, the presence of which can affect the composition of the subsurface layers of the sintered material. If carbon diffuses into the sintered material and participates in the phase formation, it leaves "footprints" in the form of carbon-containing particles (carbides) arranged in a certain pattern, which can be analysed to evaluate the significance of the carbon uptake effect on the composition and properties of the material and determine the characteristics of the spatial distribution of the newly formed phases.

A subsurface layer of certain thickness — a carbon-affected layer — is usually removed by polishing from the sintered compact and is not included in the volume of the material that is further thoroughly analysed. Therefore, little information is available on the structural and compositional changes caused by carbon diffusion into Spark Plasma Sintered specimens, especially those containing carbide-forming elements. However, a few recent studies did address the effect of carbon on the phase composition of the sintered materials. The formation of carbon-containing phases caused by carbon diffusion from the graphite paper was reported by Solodkyi et al. [2], who observed the presence of B_4C in the sintered B_6O. The B_4C phase was not found when a tantalum foil was placed between the sample and the carbon paper thus preventing carbon diffusion into B_6O. Although the presence of the carbon-containing phase was detected, its distribution in the layers of the sintered sample adjacent to the carbon foil was not studied in detail. Worth mentioning are experiments conducted by Boulnat et al. [3], who observed strengthening of the surface layer of steel samples sintered by the SPS. The W_2C phase was observed by Rodriguez-Suarez et al. [4] in the cross-sections of the compacts Spark Plasma Sintered from the

[a] *Institute of Solid State Chemistry and Mechanochemistry SB RAS, Kutateladze str. 18, Novosibirsk, 630128, Russia.*
[b] *Novosibirsk State University, Pirogova str. 2, Novosibirsk, 630090, Russia.*
[c] *Lavrentyev Institute of Hydrodynamics SB RAS, Lavrentyev ave. 15, Novosibirsk, Russia.*
† Corresponding author: Prof. Boris B. Bokhonov, Dr. Sci.,
Institute of Solid State Chemistry and Mechanochemistry SB RAS, Kutateladze str. 18, Novosibirsk 630128, Russia, tel. 7-383-233-24-10, fax 7-383-332-28-47,
E-mail: bokhonov@solid.nsc.ru
Electronic Supplementary Information (ESI) available: See
DOI: 10.1039/x0xx00000x

W-Al_2O_3 powder suggesting that carbon had diffused deep into the volume of the specimen. Zapata-Solvas et al. [5] observed the enrichment of the grain boundaries of ZrB_2 sintered in the presence of graphite foil. Microstructural indications of the processes of chemical reduction of oxide films on metallic particles in certain regions of the Spark Plasma Sintered compact were found in our recent work [6]: very fine crystallites of copper were observed on the surface of ligaments of the sintered porous copper in the areas of the compact that had been in contact with the graphite foil during consolidation.

Depending on the nature of the sintered material, carbon uptake or interaction with carbon can be undesirable, beneficial or neutral for the materials development and properties. At relatively low sintering temperatures, the presence of carbon is not an issue. In the SPS experiments with Fe-Ag and Ni-Ag composite powders consolidated at 600 °C [7], we did not encounter any problems with graphite foil's adhering to the sintered compact. However, most SPS experiments are conducted at temperatures such that the interaction with carbon cannot be neglected. Partial reduction of oxide materials by carbon during SPS leads to the formation of oxygen vacancies. In ref. [8], annealing in air was shown to be necessary to improve the infra-red transmission of the Y_2O_3-MgO nanocomposite produced by SPS though restoring the oxygen content disturbed by the presence of carbon. For certain materials, such as composites containing carbon reinforcements [9-10], the presence of carbon of the die, punch or foil is perhaps neutral in terms of influencing the target properties. An example of an advantageous in situ reduction occurring simultaneously with densification during SPS was demonstrated in ref. [11]. In that work, the in situ reduction was used as a basis for developing graphene-containing composites from graphene oxide as a starting material.

In the present study, we investigated carbidization of a Ni-15at.%W alloy during SPS in contact with graphite foil. Ni-W alloys and composites with Ni-W matrices containing ceramic inclusions have recently attracted significant attention due to their promising mechanical properties [12-17]. SPS has been shown to be a suitable technique for efficient densification of Ni-W alloy powders [16-17]. Phase and structure evolution in Ni-W-C system is an important question in the design on Ni-promoted tungsten carbide catalysts supported on activated carbon [18]. The in situ formation of Ni-WC composite layers on the surface of sintered parts can be an alternative to cladding techniques described in ref. [19]. It is important to take into account that the microstructure of composites with in situ formed carbide particles distributed in a metal matrix will depend on the distribution of the carbon source in the initial mixture [20]. In our work, the Ni-W system was studied in the context of carbon uptake during SPS for the first time. As nickel does not form thermodynamically stable carbides, the products of interaction of Ni-15at.%W alloys with carbon will not be able to form continuous layers but will be distributed in a residual Ni-based matrix as "footprints" of carbon diffusion. Therefore, this system can serve as a suitable model for studying the spatial distribution of carbide particles in a metallic alloy placed in contact with a planar source of graphitic carbon during SPS.

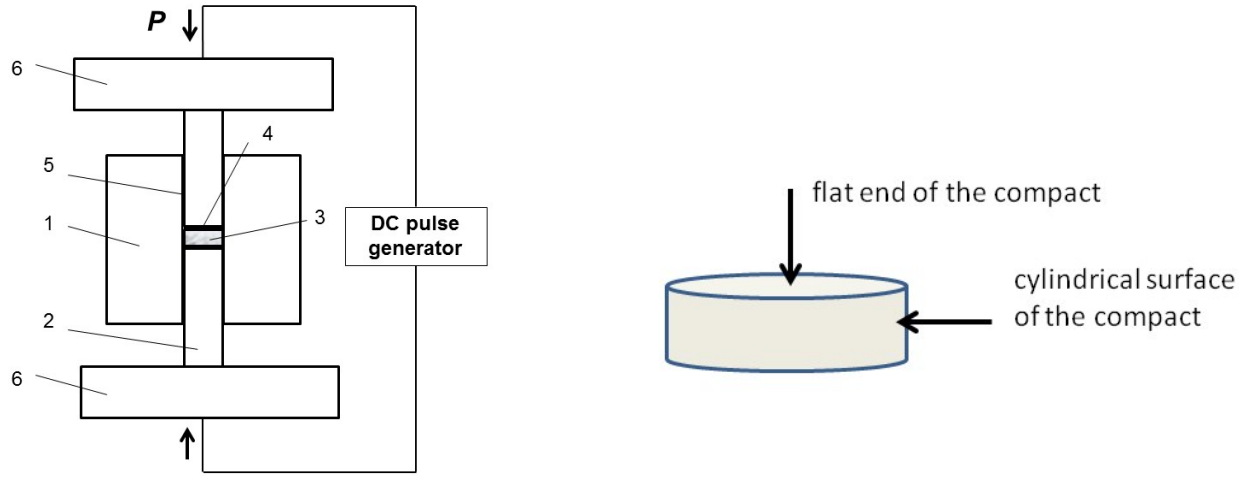

Figure 1. A schematic of the die/punch assembly used in the Spark Plasma Sintering experiments in the present work (1 – graphite die, 2 – tungsten punch, 3 – sintered disk-shaped compact (sample), 4, 5 – protective graphite foil, 6 – graphite spacers). The assembly is under forevacuum.

Materials and Methods

Carbonyl nickel powder (99.9% purity, <20 μm, Norilsk Nickel, Russia) and tungsten powder (99.5%, 0.8-1.7 μm, Polema, Russia) were mixed in a mortar to form the Ni+15at.%W mixture. The powders were mechanically milled in a high-energy planetary ball mill using a ball acceleration of 400 $m \cdot s^{-2}$ for 10-50 min in an atmosphere of argon. Stainless steel vials and balls were used. The ball to powder weight ratio was 18:1. For comparative experiments, Cu-15at.%W powders were also prepared by mechanical alloying. Electrolytic copper powder (99.7%, 40 μm, PMS-1, Russia) was used as a starting material. Another set of comparative experiments included SPS of a non-milled Ni+15at.%W mixture.

Spark Plasma Sintering of the powders was carried out using a SPS Labox 1575 apparatus (SINTER LAND Inc., Japan). The die/punch assembly (Fig.1) consisted of a graphite die of 10 mm inner diameter and 50 mm outer diameter and tungsten punches of 10 mm diameter. The die wall was lined with graphite foil 200 μm thick. The circles of the same foil were placed between the flat ends of the punches and the sample. The temperature during the SPS was controlled by a pyrometer focused on the hole in the outer wall of the die 8 mm deep at its mid-plane. The die was wrapped in graphite felt. The sample was heated at an average rate of 50 $°C \cdot min^{-1}$. The sample was held at the maximum temperature of 900 °C for 5 min and then cooled down to room temperature. The selection of the sintering temperature for the experiments was made based on refs. [16-17] reporting efficient densification of a Ni-W alloy of a composition close to the one studied in this work at 1000 °C. A possible difference between the sample real temperature and the pyrometer-measured temperature was taken into account (100 °C) for the measurement scheme used in the present work. At the beginning of the sintering cycle, a uniaxial pressure of 40 MPa was applied and kept constant through the sintering cycle. The sintered specimen was 3 mm thick (together with the circles of the graphite foil, which could be removed from the surface only by polishing).

Sintering of the Ni-W-based compact with aluminum foil was conducted to study the possible differences in the diffusion behaviour of the material relative to aluminum caused by the carbon uptake. Circles of aluminum foil 400 μm thick were cut to the size of the flat ends of the Ni-W-based sintered compact and joined with it by SPS at 500 °C using a holding time of 20 min. In this experiment, the temperature was controlled by a thermocouple inserted in the die wall. The WC-containing layer was removed from one of the flat ends on the compact and left at the other. Following SPS, the sample with adhered Al foil was annealed in vacuum for 2 h at 600 °C to increase the duration of the temperature exposure.

The phase composition of the powder and different regions of the sintered material was studied by X-ray diffraction (XRD) using Cu Kα radiation. The XRD patterns were recorded using a DRON-4 diffractometer (Russia). The microstructure of the consolidated materials was studied on the polished cross-sections of the sintered compact by Scanning Electron Microscopy (SEM) using a Hitachi-Tabletop TM-1000 and a Hitachi-3400S (Japan) Scanning Electron Microscopes. Secondary electron (SE), backscattered electron (BSE) and mixed imaging modes were used. X-ray elemental point analysis and mapping of selected regions of the polished cross-sections was carried out using an Energy Dispersive Spectroscopy (EDS) unit (NORAN Spectral System 7, Thermo Fisher Scientific Inc.) attached to the Hitachi-3400S microscope. The porosity of the compact interior and the fraction of the Ni_2W_4C particulate inclusions in the Ni-based matrix were estimated from the images of the cross-section of the sintered compact using ImageJ software (http://imagej.nih.gov/ij). Etching the polished cross-section with HCl solution (10%) was used to reveal the details of the distribution of the WC particles in the subsurface layers. Vickers hardness of the different areas of the sintered compact was measured using a DuraScan 50 hardness testing machine with a load of 0.05 kg.

Results and Discussion

The SPS experiments were conducted using the Ni-15at.%W powder mixture mechanically milled for 50 min. The morphology of the powder particles is shown in Fig.2 (a). The evolution of the XRD patterns of the mixture with milling time (from 10 to 50 min) showed that refinement of the crystallite size as well as alloying became more pronounced as the milling continues (Fig.1S). The reflections of the f.c.c. Ni(W) solid solution gradually shifted to lower angles indicating an increase in its lattice parameter caused by continuous dissolution of tungsten — a metal with a larger atomic radius — in the nickel matrix (r_{Ni}=0.125 nm, r_W=0.141 nm [21]). The powder milled for 50 min consisted of a Ni(W) solid solution and a small amount of residual metallic tungsten both having a nanocrystalline structure, as can be inferred from the very broad XRD reflections. The XRD pattern of the Ni-15at.%W powder mixture prepared by mixing in a mortar is given as a reference in Fig.2 (b). The analysis of the phase composition of the sintered compact showed that carbon diffusing from the foil into the Ni-15wt.% W compact during sintering participated in the phase formation of the consolidated material. The XRD patterns from the flat ends of the sintered compact were taken after the circles of the adhered graphite foil had been removed by mild polishing. As can be seen from the the XRD pattern, tungsten carbide WC forms in the subsurface layers of the compact (Fig.2 (b)). The formation of tungsten carbide according to the following reaction

$$Ni(W) + C = WC + Ni, \quad (i)$$

is accompanied by a shift of the $Ni_{s.s.}$ reflections to higher angles, which indicates a reduced concentration of tungsten in the remaining solid solution. The reflections are marked $Ni_{s.s.}$ to note the fact that traces of both carbon and tungsten can be still present in the dissolved state in the nickel matrix, as the positions of the reflections are still shifted relative to those of the starting nickel powder. The XRD pattern taken from the cross-section of the sintered compact parallel to the pressing direction shows the presence of the reflections of Ni_2W_4C, which can form in the conditions of carbon deficit. For clarity

of the phase composition of the compact interior, the XRD pattern obtained from the cross-section parallel to the flat ends of the sample (normal to the pressing direction) at a distance of 1 mm from the interface with the graphite foil is shown in Fig.2 (c). The presence of the reflections of Ni_2W_4C in the XRD pattern taken from the interior of the sample shows that tungsten carbide WC is not the only product of interaction of carbon with the metallic components of the alloy. We can assume that during sintering, the carbon concentration gradient is established such that the concentration of carbon in the interior is still sufficient for the Ni_2W_4C phase to form. This phase was observed by Fabičovicová et al. [22] during the preparation of Ni-W-activated carbon catalysts and by Hu et al. [23], who Spark Plasma Sintered W-Ni-Fe alloys from mechanically milled powders. In ref. [23], the milling was carried out using tungsten carbide balls, so the powders already contained a certain amount of WC introduced as contamination during milling, which made it difficult to estimate the contribution of carbon introduced in situ during SPS to the resultant phase composition of the sintered material. The formation of the Ni_2W_4C phase in the compact's interior was also confirmed by SPS experiments with the non-milled Ni+15at.%W powder. Broader reflections of the Ni-based matrix in the WC-containing layer compared with the interior (Fig.2 (b)) is likely to be due to crystallite growth retardation by carbon dissolved in nickel [24], which is present in the subsurface layer in the form of interstitial solute atoms in higher concentrations than in the interior.

The "footprints" left by the carbon flux — the microstructural consequences of the carbon diffusion in the direction of the compact interior — can be seen in the images of the cross-section of the sintered compact (Fig.3). The interface between the graphite foil and the sintered compact is shown in Fig.3 (a). The presence of the foil lining the wall of the die led to the formation of a carbide-containing layer on the cylindrical surface of the sample, while the circles of the foil between the punches and the sample caused the formation of layers with an altered composition at the top and bottom surfaces — flat ends of the disk-shaped compact. The thickness of this layer was the same for the top and bottom flat ends of the sample — about 100 μm (Fig.3 (b)), and, consequently, did not depend on the direction of the electric current applied during sintering relative to alloy/carbon interface. The layer on the cylindrical surface of the compact has a structure similar to that found at the flat ends of the sample in terms of the distribution character of tungsten carbide particles, but is thinner — 50-70 μm (Fig.3 (c)). Fig.3 (d) demonstrates the boundary between the WC-containing layer and the interior of the compact. This boundary is generally parallel to the interface between the foil and the compact, but in several locations shows a wavy geometry. Interestingly, when pure molybdenum was sintered by SPS in contact with carbon foil, a carbide phase — β-Mo_2C — also formed a continuous layer with a wavy boundary with the Mo interior [25]. This similarity in the geometry of the boundary of the layers formed as a result of carbon uptake by the samples points to the dependence of the carbon diffusion on the geometrical parameters of the particles of the material that is sintered: in the case of molybdenum — on the grain size of molybdenum and in the present study — on the size of the Ni-W powder agglomerates formed by mechanical milling.

It can be seen from Fig.3 (b, d) that particles of WC observed at depths of 20-50 μm from the interface are smaller than those observed at a depth of 100 μm, which is possibly due to a higher concentration of carbon in the areas located closer to the interface with the foil favouring nucleation of the WC phase. The particles located 80-100 μm from the interface are 1-2 μm in size; they are well crystallized and prism-shaped. EDS taken from an area in the cross-section covering the graphite foil and a WC-containing layer at one of the flat ends of the compact is provided in Fig.2S. The concentration profiles of the elements obtained by measurements starting at the foil and continuing through and beyond the WC-containing subsurface layer in the direction normal to the compact/foil interface are consistent with the observed phase composition of the sintered material and show that carbon is also present in regions lying beneath the subsurface layer (Fig.3S). Iron and chromium are present in the sintered compact due to contamination from the material of the milling balls introduced during prolonged mechanical milling of the powder.

In order to reveal further details of the distribution of the WC particles in the subsurface layers of the compact, the polished cross-section of the compact was etched with HCl solution. EDS mapping of WC particle-containing regions is presented in Fig.4S. As is seen from Fig.4 (a), a fraction of WC particles is organized in chains clearly visible in the microstructure. Particles forming these chains are less than 1 μm in size. The distribution of larger particles embedded in the metal matrix does not follow any pattern. The correspondence of the bright particles in the images to the WC phase is confirmed by the EDS point analysis (Fig.4 (c)). The chains formed by the submicron particles appear to be a feature structurally "inherited" from the powder state of the Ni-15at.%W alloy. Indeed, the size of regions encircled by the chains (Fig.4 (b)) is comparable to the size of the powder particles present in the mechanically milled mixture (Fig.2 (a)). Different materials are known to allow the flux of carbon atoms to pass thanks to the grain boundary mobility of carbon [26]. In the present work, the paths for faster diffusion are offered by boundaries between the initial powder agglomerates, the latter being composed of many grains.

The image shown in Fig.5 (a) is representative of the microstructure of the interior of the Ni-W-based compact. The porosity of the central part of the compact estimated from the images of the cross-sections is less than 1 %. Bright particles smaller than 1 μm (Fig.5 (b)) clearly distinguishable on a darker background correspond to the Ni_2W_4C phase, as can be concluded by analyzing the XRD and SEM data. The fraction of the Ni_2W_4C particles in the Ni-based solid solution matrix estimated from the images is 1 vol.%. In the distribution of Ni_2W_4C particles, a pattern is visible (Fig.5 (a)), which is similar to that of the distribution of submicron WC particles in the subsurface layers of the compact. There are areas with higher

concentrations of the Ni_2W_4C particles and those practically particle-free. The Ni_2W_4C particles and submicron particles of WC form networks, which, from a geometrical point of view, correspond well to the boundaries between the agglomerates of the mechanically milled powder consolidated by solid-state sintering into a compact by SPS. The feature of fast solid-state sintering is that even in a nearly fully dense material, the boundaries between the initial powder particles remain structurally different from their volume [27]. In the present case, the boundaries are different from the volume of the agglomerates formed by cold-welding during mechanical milling and offer paths for faster diffusion of carbon favouring the formation of carbide nuclei along them. It can be also assumed that diffusion of carbon occurred faster along the surface of the powder particles not yet fully consolidated into a bulk material upon heating during the SPS. This leads us to a conclusion that the character of distribution of the carbon-containing compounds — both WC and Ni_2W_4C — is to a great extent predetermined by the particle size and morphology of the mechanically milled powder.

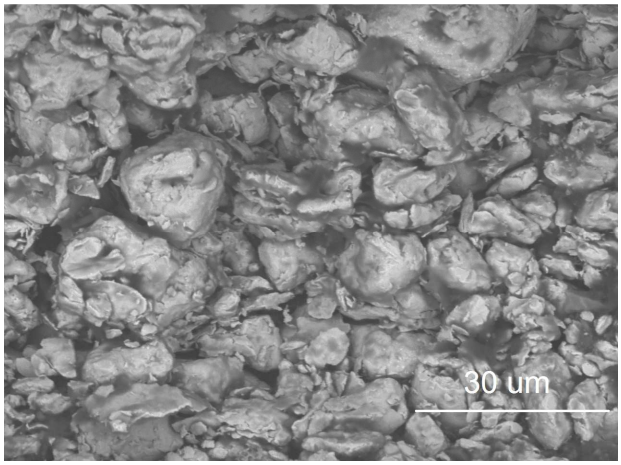

a

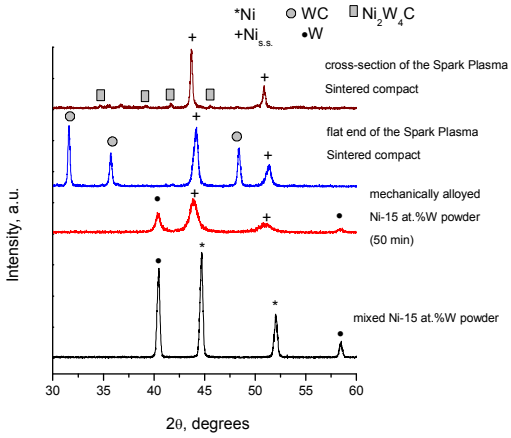

b

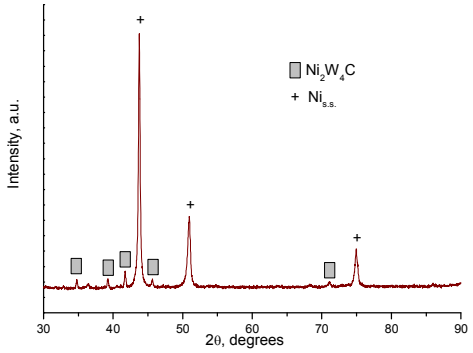

c

Figure 2. Morphology of the Ni-15at.%W powder mechanically milled for 50 min (a), XRD patterns of the Ni-15at.%W powder mixture prepared by mixing in a mortar, mechanically alloyed powders (milling time 50 min), flat end of the Spark Plasma Sintered compact that was in direct contact with the graphite foil and cross-section of the sample parallel to the pressing direction (b), XRD pattern of the compact obtained from the cross-section parallel to the flat ends of the sample (normal to the pressing direction) at a distance of 1 mm from the interface with the graphite foil (c).

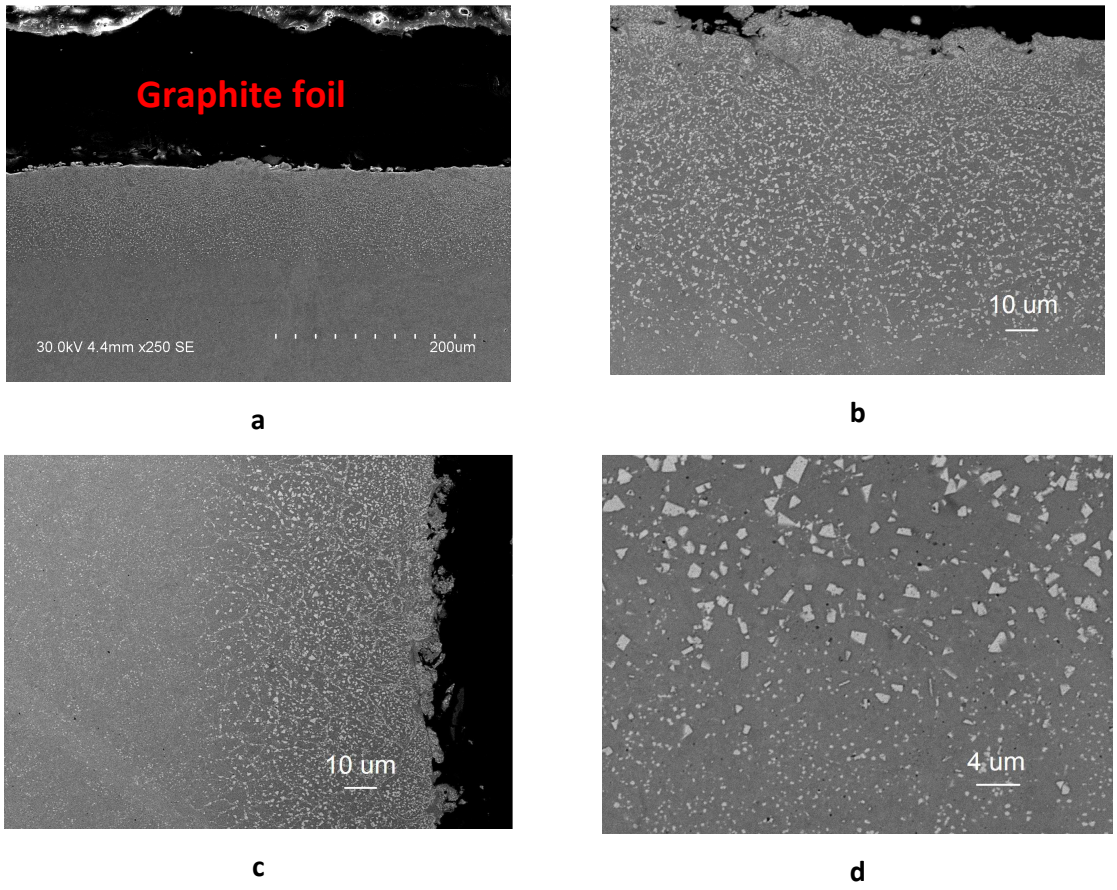

Figure 3. Cross-sectional views of the compact Spark Plasma Sintered from the Ni-15at.%W powder in contact with graphite foil: (a) general view, (b) WC-containing layer at the flat ends of the compact, (c) WC-containing layer on the cylindrical surface of the compact, (d) boundary between the WC-containing layer and the interior of the compact ((a) SE image, (b-d) BSE images).

The thickness of the carbon diffusion zone depends on the diffusivity of carbon in the sintered material and sintering temperature. Noteworthy is the experiment described in ref. [28], which showed that only a thin layer of titanium carbide TiC — 10 μm thick — forms on a flat surface of a metallic titanium plate treated in the SPS for 1 h with carbon powder poured into the sintering die. Based on the activation energy determined for the process, it was concluded that the inward diffusion of carbon in TiC is the rate-controlling process. Diffusion of carbon from the graphite punch into the surface of the sample during SPS was used to restore carbon in thermally sprayed WC-based coatings that had lost some carbon during spraying and contained the W_2C phase [29-30]. A layer of the plasma sprayed WC-Co coating, in which the carbon content was restored, was less than 10 μm thick for the SPS treatment time of 6 min and a temperature of 800 °C [30]. For the case of the Ni-15at.%W alloy placed in contact with carbon, it is the diffusion of carbon in the Ni-based matrix that needs to be considered. In order to calculate the thickness of the carburised layer obtained at a pyrometer-measured temperature of 900 °C, we should perform calculations for a higher temperature (1000 °C), as the temperature in the electrically conducting sample is normally higher than that measured by a pyrometer on the die wall during SPS [31]. The volume diffusion coefficient of carbon in nickel is $3 \cdot 10^{-7}$ $cm^2 \cdot s^{-1}$ at 1000 °C [32], so, assuming the concentration of carbon at the interface constant, the thickness of the carburized layer x, cm, can be estimated as follows:

$$x \sim (Dt)^{1/2}, \quad (1)$$

where D is the diffusion coefficient, $cm^2 \cdot s^{-1}$ and t is time, s. At 1000 °C, x is of the order of 100 μm, which agrees well with the observed thicknesses of the WC-containing subsurface layers in the sintered sample. It should be kept in mind that this thickness was calculated for a 50% drop in the carbon concentration relative to the concentration at the interface using the volume diffusion coefficient. The presence of carbon in the sintered material should also be taken into account at greater distances from the interface due to much faster (orders of magnitude) diffusion along the surface of pores and grain boundaries during sintering.

A comparative experiments with a Cu-15at.%W alloy produced by mechanical alloying showed that it is not the

presence of the carbide-forming element that determines the character of interaction of the graphite foil with the sintered material and the microstructure of the interfacial regions of the sintered compact, but the solubility of carbon in the component that plays the role of a matrix in the sintered material. Indeed, no tungsten carbide-containing layer formed when the Cu-15at.%W powder was Spark Plasma Sintered in the same conditions. Instead of a carbide-containing layer adjacent to the graphite foil, we observed a uniform microstructure through the thickness of the sintered compact (Fig.5S). This difference can be explained by a significantly higher solubility of carbon in nickel compared to copper.

The hardness of the interior of the sintered compact consisting of a Ni-based matrix and Ni_2W_4C inclusions (Table 1) is comparable to that of the nanocrystalline Ni-W alloys [13] indicating a successful outcome of the SPS-procedure. A high hardness of this composite is a result of efficient densification (estimated porosity less than 1 %, as was noted above), the presence of Ni_2W_4C particles in the Ni-based matrix and solid solution strengthening of nickel by tungsten and carbon. Despite the presence of WC particles in the Ni-based matrix, the hardness at distances 20-50 μm from the interface with the graphite foil is lower than that of the layers located deeper and the sample's interior (Table 1, Fig.6S). A lower hardness appears to be related to incomplete densification (the presence of residual porosity) of the subsurface layers of the material experiencing higher transformation degrees of tungsten into its carbide. Macrodefects are present in a thin subsurface layer of the compact adjacent to the graphite foil (Fig.3 (b-c)). This layer is only 10-20 μm thick. As the Ni-W powder was not cold-pressed before SPS but simply poured into the die, which was then tapped to flatten the surface of the sample, a circle of the graphite foil, when placed in contact and pressed to the powder compact, could disturb the surface particles of the powder causing these defects in the sintered specimen. Similarly, such defects form on the cylindrical surface of the sintered specimen. Normally, in the practice of SPS, this layer is removed from the sintered compacts together with the pieces of adhered graphite foil by polishing. In our work, we kept the foil adhered to the sample to show the microstructure of the layer of the sintered compact affected by carbon diffusion.

Surface carbidization of alloys offered by the SPS technique can be of practical importance. Ni-based alloys containing tungsten are often coated with aluminides to improve their corrosion resistance. When an Al-containing coating is applied to a part made of a Ni-based alloy, topologically close-packed phases are likely to form in Al-rich areas. These phases lead to deterioration of the mechanical properties of the material. Following ref. [33], the formation of these phases can be avoided if tungsten is bound into its carbide WC. In the present study, we have evaluated the behaviour of the SPS-consolidated Ni-W-based material during interdiffusion in contact with an aluminum layer. The WC-containing layer was removed from one flat side of the compact and kept at the other with minor polishing applied to obtain a flat surface. The Al foil was joined with the Ni-W-compact during SPS, but the time (20 min) that was used was insufficient for observing the interdiffusion results by microstructural changes. During further annealing at 600 °C, interdiffusion layers with dramatically different structures formed at the two flat ends of the Ni-W-based compact (Fig.6). The interdiffusion behaviour of the pair, in which the WC-containing layer participated, was pre-determined by a reduced concentration of tungsten in a metallic state (Fig.6 (a-b)). At the other side, where the WC-containing layer was removed, a characteristic periodic pattern of alternating layers (Fig.6 (c-d)) rich in W (Fig.6 (e) and rich in Ni (Fig.6 (f)) formed. The formation of periodic structures by interdiffusion between Ni-W solid solutions and Al has been demonstrated and theoretically explained by Oberhauser et al. [34]. The formation of W-rich and Ni-rich layers imply diffusional mobility of tungsten in the metallic phase of the Ni(W)-Ni_2W_4C composite enabling its re-distribution when brought in contact with aluminum. Such mobility was obviously not characteristic of the WC-containing layer.

In the present study, we showed for the first time that layers located at different distances from the interface with the graphite foil can vary in the phase composition and the composition of the carbide phase itself. The geometry of the sample and its size determine the fraction of the sample volume affected by carbon diffusion. The local temperatures developing during sintering and the direction of electric current relative to the graphite foil/sample interface are possible factors that influence the microstructure development and the thickness of the layers affected by carbon diffusion. The thicknesses of the affected layers may be different at the flat ends and on the cylindrical surface of disk-shaped samples normally processed by SPS. The results of this study showed that carbon diffusion into the sintered sample can affect the phase composition of not only the subsurface regions, but also the interior of the sample at the millimeter scale. Taking into account fast diffusion of carbon during SPS is especially critical for nanostructured systems and powders with high defect concentrations, such as mechanically milled powders, which are widely used as starting materials in the practice of consolidation and solid-state synthesis by SPS. In addition, the effect of carbon uptake deserves a special consideration when the SPS processing is scaled-up to industrial scale. Therefore, laboratory research of this issue should be continued and extended for other technologically important materials.

High flexibility of electric current-assisted sintering techniques in terms of the treatment conditions, sample size/shape and sample state (powder or pre-consolidated) has encouraged researchers to use those not only for making bulk specimens from powders, but also for joining different materials and applying coatings [25, 28, 35-37]. Surface modification of the sintered specimen can be based on applying a layer of a material chemically different from the main sintered body. This was done by placing a powder bed on a flat solid substrate followed by sintering. In refs. [38-39], it was shown that the surface of the sintered specimen can differ in composition from that of the core, if the material is chemically sensitive to the reducing environment. Our studies

have demonstrated that the inherent design of the SPS can cause the formation of sintered compacts with modified surfaces.

As far as substitutes for graphite foil are concerned, none of the so far attempted materials has proven satisfactory for the needs of SPS, which normally aims at the fabrication of contamination-free sintered materials. The protective foil should not cause disruption of electric current. At the same time, it should be easy removable from the surface of the compact after the experiments. In our studies, tantalum foil was used to protect the flat ends of tungsten punches from the action of the sintered nickel-diamond material at elevated temperatures, but the formation of TaC at the interface could not be avoided [40]. It was also rather difficult to tear the circle of the foil off the sintered compact. An attempt was made to use copper foil to protect porous iron compacts from carbon contamination. The foil served this purpose quite well in pressure-less SPS experiments, but was not suitable for sintering at temperatures exceeding 800 °C.

At present, alternative materials for SPS dies are being sought. One of the possible solutions has been suggested by Kakegawa et al. [41], who studied the SPS process in silicon carbide dies. The experiments proved to be successful provided additional heating is imposed on the SiC die (from external heaters) in the beginning of a pulsed current sintering process to increase the electrical conductivity of SiC. Further research and development activities in this direction will broaden the range of conditions achievable in the SPS and similar advanced sintering and solid-state synthesis facilities.

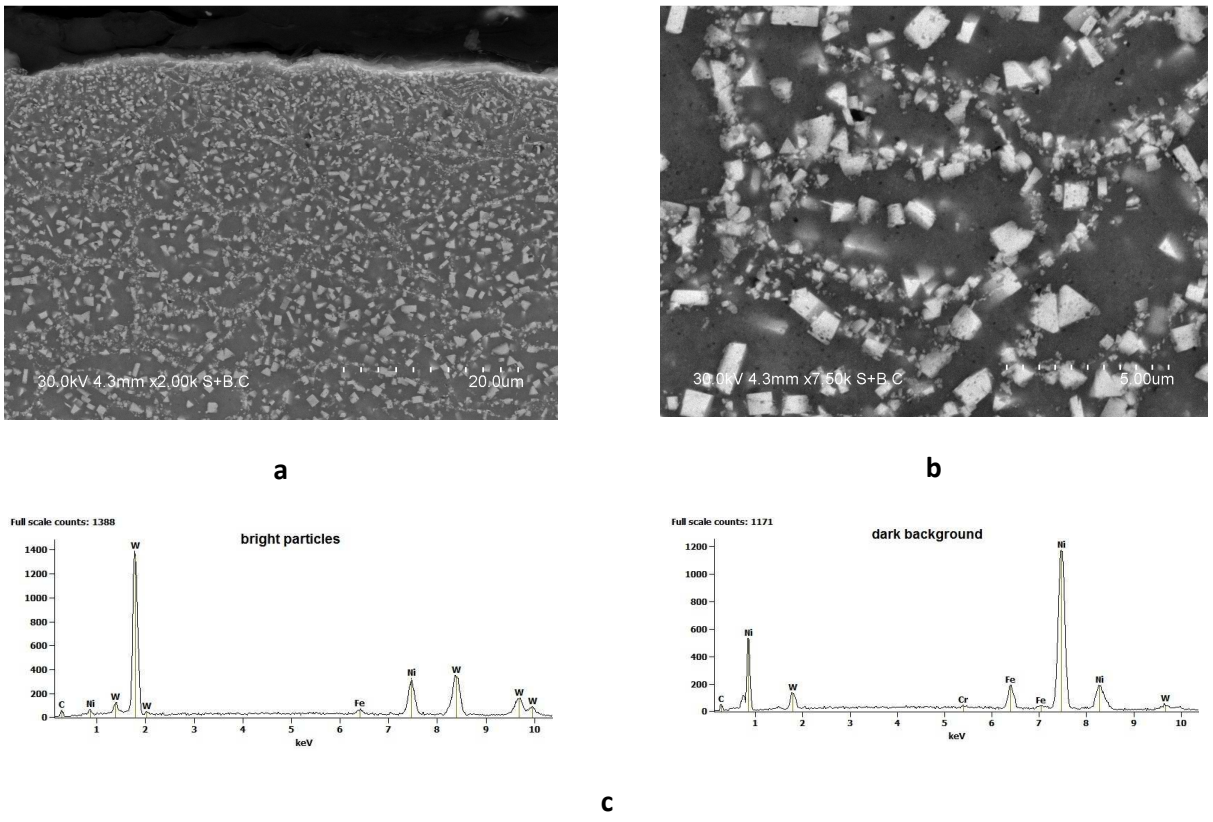

Figure 4. Subsurface layer of the compact Spark Plasma Sintered from the Ni-15at.%W powder in contact with graphite foil (at the flat end) etched in 10% HCl solution: (a) WC-containing layer adjacent to the graphite foil, (b) microstructure details at a distance of 30 µm from the interface with the graphite foil, (c) EDS taken from the bright particles and dark background.

Table 1. Vickers hardness of different areas of the compact Spark Plasma Sintered from the Ni-15at.%W powder in contact with the graphite foil.

Area of the cross-section	Distance from the interface with the graphite foil to the measurement point, μm	Vickers hardness, HV
Flat ends of the compact	20-50	470±10
	50-100	610±10
	100-150	620±10
Cylindrical surface	20-30	510±10
	30-70	620±10
	70-120	650±10
Interior of the compact	500-1000	620±10

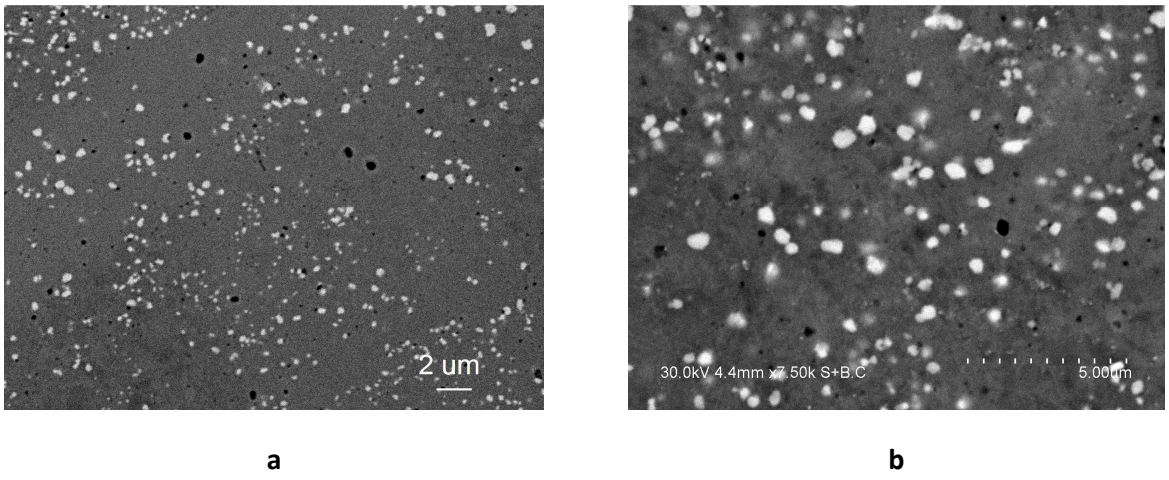

a b

Figure 5. The interior of the compact Spark Plasma Sintered from the Ni-15at.%W powder in contact with the graphite foil: (a) the distribution character of the Ni_2W_4C particles and (b) a higher-magnification view of an area rich in Ni_2W_4C particles (BSE images).

Conclusions

We have investigated the phase formation and microstructure development during Spark Plasma Sintering of a Ni-15at.%W alloy placed in contact with graphite foil. A tungsten carbide WC-containing layer about 100 μm thick formed at the flat ends of the cylindrical sample, which were in direct contact with the foil during sintering. The subsurface layer on the cylindrical surface of the sample was thinner (50-70 μm) but had a structure similar to that at the flat ends of the sample in terms of the distribution character of the WC particles. The analyses showed that it was not only the subsurface layer of the sample that was affected by carbon diffusion: the Ni_2W_4C phase formed at greater distances from the interface in the conditions of carbon deficit and was found throughout the thickness of the sintered compact. The distribution of the submicron WC particles and Ni_2W_4C particles in a metal matrix had a chain-like pattern following a network of boundaries between the agglomerates of the mechanically milled powder solid-state consolidated by SPS. A lower hardness of the very subsurface layers of the sintered material was due to incomplete densification of regions with high transformation degrees of tungsten into WC. The carbidization of the Ni-W alloy changed not only the microstructure of the subsurface layers but also the chemical reactivity of the material towards aluminum. The interdiffusion between the carbide subsurface layer and aluminum foil differed dramatically from that between the interior of the compact and aluminum due to a significantly reduced concentration of tungsten capable of diffusing within a metallic phase in the former. A comparative experiments with a Cu-15at.%W alloy showed that it is not the presence of the carbide-forming element that determines the character of interaction of the graphite foil with the sintered material, but the solubility of carbon in the component of the alloy playing the role of a matrix.

Acknowledgements

This work was partially supported by the Ministry of Education and Science of the Russian Federation (contract 14.604.21.0013).

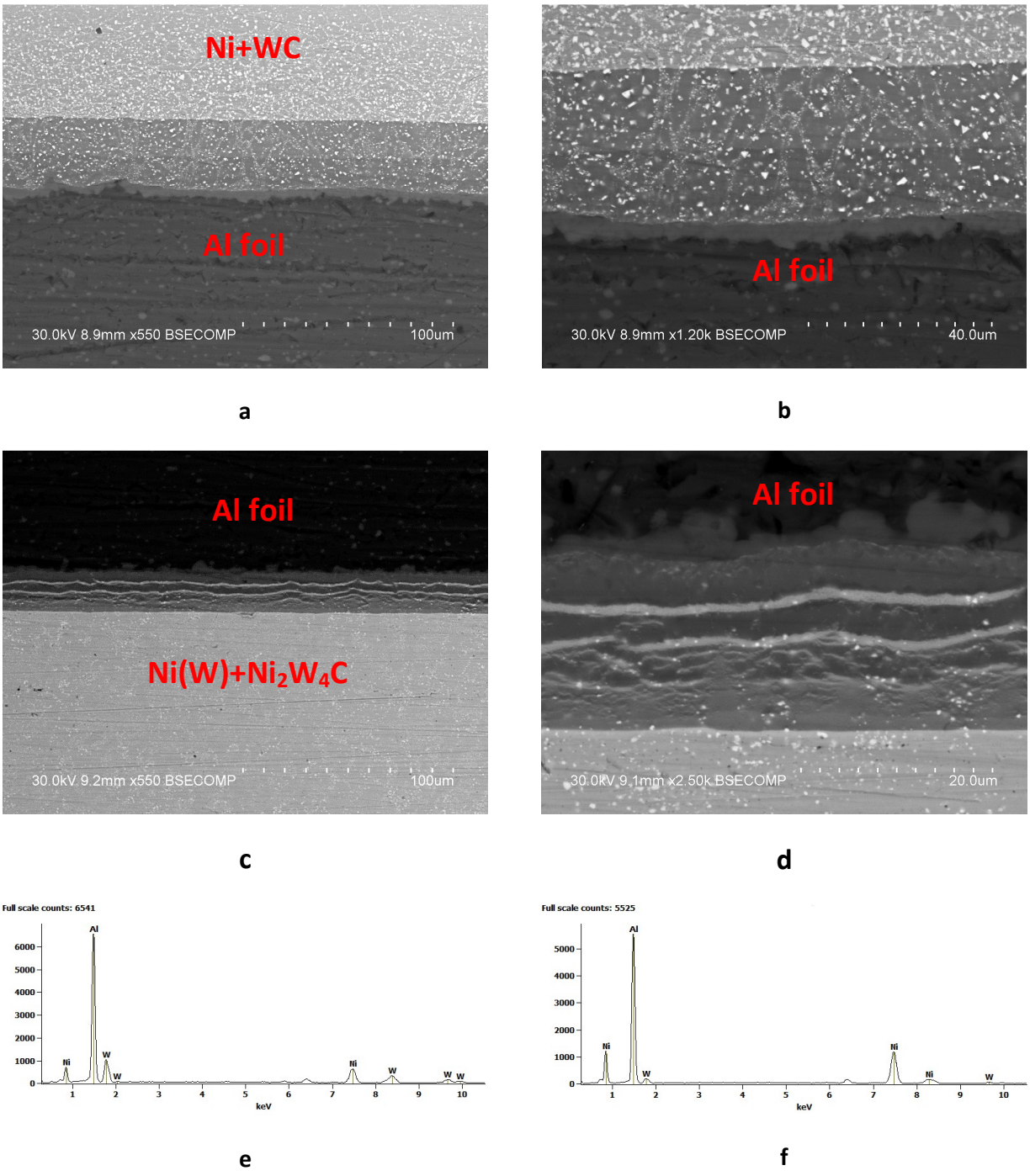

Figure 6. Cross-sectional views of the interdiffusion zone formed between an Al foil and flat ends of the Spark Plasma Sintered Ni-W-based compact after additional SPS treatment at 500 °C for 20 min and vacuum annealing at 600 °C for 2 h: (a-b) the carbide layer was kept on the compact after SPS with the graphite foil, different magnifications, (c-d) the carbide layer was removed, different magnifications, (e) EDS from a bright layer of the interdiffusion zone shown in (c-d), (f) EDS from a dark layer of the interdiffusion zone shown in (c-d).

Notes and references

1 Z. A. Munir, D. V. Quach, M. Ohyanagi, *J. Am. Ceram. Soc.*, 2011, **94**, 1.
2 I. Solodkyi, S. S. Xie, T. Zhao, H. Boridianska,Y. Sakka and O. Vasylkiv, *J. Ceram. Soc. Japan*, 2013, **121**, 950.
3 X. Boulnat, D. Fabrègue, M. Perez, S. Urvoy, D. Hamon and Y. de Carlan, *Powder Metall.*, 2014, **57**, 204.
4 T. Rodriguez-Suarez, L.A. Díaz, R. Torrecillas, S. Lopez-Esteban, W.-H. Tuan, M. Nygren and J.S. Moya, *Comp. Sci. Technol.*, 2009, **69**, 2467.
5 E. Zapata-Solvas, D. Gómez-García, A. Domínguez-Rodríguez, and R. I. Todd, *Sci. Rep.*, 2015, **5**, 8513.
6 D. V. Dudina, A. G. Anisimov, V. I. Mali, N. V. Bulina and B. B. Bokhonov, *Mater. Lett.*, 2015, **144**, 168.
7 B. B. Bokhonov and D. V. Dudina, *RSC Adv.*, 2013, **3**, 12655.
8 D. Jiang and A. K. Mukherjee, *Scripta Mater.*, 2011, **64**, 1095.
9 P. Wang, W. Liu, L. Chen, C. Mu, G. Qi and F. Bian. *RSC Adv.*, 2015, **5**, 51342.
10 K. Ahmad, W. Pan and H. Wu, *RSC Adv.*, 2015, **5**, 33607.
11 C. Ramírez, S. M. Vega-Diaz, A. Morelos-Gómez, F. M. Figueiredo, M. Terrones, M. Isabel Osendi, M. Belmonte and P. Miranzo, *Carbon*, 2013, **57**, 425.
12 C.A. Schuh, T.G. Nieh and H. Iwasaki, *Acta Mater.*, 2003, **51**, 431.
13 A. J. Detor and C. A. Schuh, *Acta Mater.*, 2007, **55**, 371.
14 Y. Boonyongmaneerat, K. Saengkiettiyut, S. Saenapitak and S. Sangsuk, *Surf. Coat. Technol.*, 2009, **203**, 3590.
15 S. Yari and C. Dehghanian, *Ceramics Intl.*, 2013, **39**, 7759.
16 A. Genc, E. Ayas, M. Lütfi Övecoqlu and S. Turan, *J. Alloys Comp.*, 2012, **542**, 97.
17 A. Genc, P. Kaya, E. Ayas, M. Lütfi Övecoglu and S. Turan, *J. Alloys Comp.*, 2013, **571**, 159.
18 C. B. Rodella, D. H. Barrett, S. F. Moya, S. J. A. Figueroa, M. T. B. Pimenta, A. A. S. Curvelo and V. Teixeira da Silvad, *RSC Adv.*, 2015, **5**, 23874.
19 P. Farahmand, S. Liu, Z. Zhang and R. Kovacevic, *Ceramics Intl.*, 2014, **40**, 15421.
20 S. Li, B. Sun, H. Imai and K. Kondoh, *Carbon*, 2013, **61**, 216.
21 Smithells Metal Reference Handbook, Eds. E. A. Brandes and G. B. Brook, 7th Edition, Butterworth-Heinemann, 1998.
22 K. Fabičovicová, O. Malter, M. Lucasa and P. Claus. *Green Chem.*, 2014, **16**, 3580.
23 K. Hu, X Li, D. Zheng and Y. Li, *Rare Metals*, 2011, **30**, 581.
24 S. Latif, M. Mehmooda, J. Ahmad, M. Aslam, M. Ahmed and Z. Zhang, *Appl. Surf. Sci.*, 2010, **256**, 3098.
25 B. Mouawad, M. Soueidan, D. Fabrègue, C. Buttay, V. Bley, B. Allard and H. Morel, *Metall. Mater. Trans. A*, 2012, **43**, 3402.
26 L. A. Hayden and E. Bruce Watson. *PNAS*, 2008, **105**, 8537.
27 D. L. Zhang, *Progress Mater. Sci.*, 2004, **49**, 537.
28 T. Hayashi, K. Matsuura and M. Ohno, *Mater. Trans.*, 2013, **54**, 2098.
29 L. G. Yu, K. A. Khor, H. Li, K.C. Pay, T. H. Yip and P. Cheang, *Surf. Coat. Technol.*, 2004, **182**, 308.
30 H. Li, K. A. Khor, L. G. Yu and P. Cheang, *Surf. Coat. Technol.*, 2005, **194**, 96.
31 K. Vanmeensel, A. Laptev, J. Hennicke, J. Vleugels and O. Van der Biest, *Acta Mater.*, 2005, **53**, 4379.
32 J. J. Lander, H. E. Kern and A. L. Beach, *J. Appl. Phys.*, 1952, **23**, 1305.
33 J. C. Schaeffer, *US Patent* 5 334 263, 1994.
34 S. Oberhauser, Ch. Strobl, G. Schreiber, Ch. Wuestefeld and D. Rafaja, *Surf. Coat. Technol.*, 2010, **204**, 2307.
35 W. Liu and M. Naka, *Scripta Mater.* 2004, **48**, 1225.
36 J. Yang, J. Trapp, Q. Guo and B. Kieback, *Mater. & Design,* 2013, **52**, 179.
37 E. G. Grigoryev, L. Yu. Lebedeva, O. L. Khasanov and E. A. Olevsky, *Adv. Eng. Mater.*, 2014, **16**, 792.
38 J. Gurt Santanach, C. Estournès, A. Weibel, A. Peigney, G. Chevallier and Ch. Laurent, *Scripta Mater.*, 2009, **60**, 195.
39 J. Gurt Santanach, C. Estournès, A.Weibel, G. Chevallier, V. Bley, C. Laurent and A. Peigne, *J. Eur. Ceram. Soc.*, 2011, **31**, 2247.
40 B. B. Bokhonov, A. V. Ukhina, D. V. Dudina, K. B. Gerasimov, A. G. Anisimov and V. I. Mali. *RSC Adv.,* 2015, **5**, 51799.
41 K. Kakegawa, C. M. Wen, N. Uekawa and T. Kojima, *Key Eng. Mater.*, 2014, **617**, 72.